Sub-Optimal Control Law for Active Magnetic Bearings Suspension

G. Barbaraci[#1], G. Virzì Mariotti[#2]

Universita' di Palermo. Dipartimento DICGIM, Viale delle Scienze, 90128 Palermo, Italy

[1]gabriele.barbaraci@unipa.it

[2]gabriele.virzimariotti@unipa.it

***Abstract*-This paper deals with the comparison of three types of sub-optimal control law for the stable levitation of a turbojet shaft, sustained by two radial active magnetic bearings (AMBs). Shaft is considered rigid for the procedure simplification. The utilized approach leads to development of different sub-optimal control laws to use in speed-varying simulations in the angular speed of the shaft. The first control matrix is obtained by explicit relationships of the parameters of the control law vs. speed, obtained using a curve-fitting procedure neglecting the speed-varying elements out of the main diagonal of each single block constituting the entire control matrix. The second control law is obtained by control matrix set to zero angular speed during speed-varying simulations. The third control matrix is obtained by the second neglecting the elements out of main diagonal. Time response to the step input shows difference in performance of the AMBs when varying the control law. All control laws are tested by means of simulation. The study allows showing like a polynomial representation of the control matrix, developed to the variation of angular speed, is able to maintain stable the magnetic levitation.**

Keywords-Optimal control, Sub Optimal control, active magnetic bearing, turbojet shaft, closed loop.

I. INTRODUCTION

The system considered in this paper consists of a floating mechanical rotor and three active magnetic bearings (AMBs), two radial and one axial, which provide suitable controlled dynamic forces, thus allowing the suspended object to display a stable motion.

Due to the contact-less operation capability, the AMB system has many promising advantages for high-speed, high-temperature, and clean environment applications. Moreover, adjustable stiffness capabilities and damping characteristics also make the AMB suitable for elimination of vibrations. Although the system is complex and considered an advanced topic in terms of its structural and control design, the advantages that it offers compensate for the design complexity.

Application areas of magnetic bearings are still steadily expanding. Some AMB applications that have received many attentions [22] by many research groups are the flywheel energy and storage device [1]-[2], the turbo molecular pump [3], compressors [4], the Left Ventricle Assist Device (LVAD) [5] and the artificial heart [6], [7], [8].

Magnetic bearing systems are designed in a few configurations to satisfy various specifications that arise from different applications. The rotor can be oriented in horizontal and vertical positions; in both positions, the effect of gravity is decoupled from the system dynamic forces and, consequently, the vertical displacement is controlled separately from the other set of magnetic coils controlling horizontal position [3], [9].

The magnetic bearing system consists of a rotor in the horizontal orientation. However, it is, more widely used. Moreover, in some applications, such as the artificial heart, the rotor is oriented in both the horizontal and vertical positions, due to the nature of operations depending on the position and movement of the host [7], [8].

The design of magnetic bearings is carried out utilizing suitable methodologies. Often, a linear model of these actuators is used to approximate the nonlinear relationship between force, current, and air gap length, thus obtaining a model suitable for the design of linear controllers.

A disadvantage of this approach is that the linear model is approximated around a single operating point, and the validity of this model decreases as the physical system is perturbed from this point.

This approach has been previously considered for an AMB system in [10]. Other related approaches, such as input–output linearization [11] [12] have also been examined. In [13], experimental results from a one-degree-of-freedom AMB are given. In [14] a control law is derived and tested experimentally. In particular, it is shown that instability phenomena on rotor positions can exist due to coupling effects that result from the elements of the control matrix. The rotor dynamic modelling and experimentally extracted transfer functions are presented and analysed in the paper [21], [22].

However, if good feedback control is designed, the variations of the mechanical variables, such as the displacements of the shaft within the air gap between stator and rotor can be always kept very small and, consequently, the above linearization approach yields valid results.

A stable electromagnetic suspension system may be obtained by means of state feedback optimal control. Because a turbojet shaft is subjected to angular speed variations during operations, a speed-varying control law is necessary. This control law should be obtained by solving, on-line, the matrix Riccati equation for each value of the angular speed, but this requires considerable computational efforts.

DOI 10.5963/JCET0201001

The contribution of this paper compared to the previous is in the fact that the speed-bearing optimal control law is obtained by solving, off-line, the matrix Riccati equation for each value of the angular speed, thus obtaining a set of gain matrices. In succession, the analytical expressions of all the elements of these gain matrices vs. the shaft speed are determined using a curve-fitting procedure. Several simulation tests carried out on a closed-loop system consisting of the rotating shaft and the AMBs show that this optimal control law, figured in polynomial matrix form, can support the rotor at every value of the angular speed in presence of both static and harmonic loads. No experimental parts are introduced with the present paper, because the experimental tests were executed in the paper [24], with the purpose to validate the theory presented in this paper.

Hypothesis of rigid rotor is done due to the simplicity of the analysis; computational analysis of flexible rotor configuration has been left out for future developments in this field.

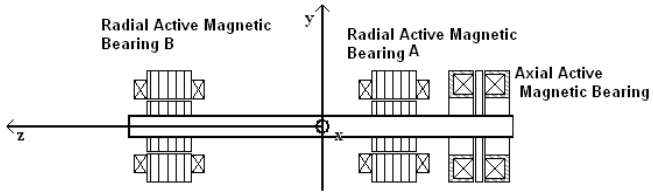

Fig. 1 Active Magnetic Suspension

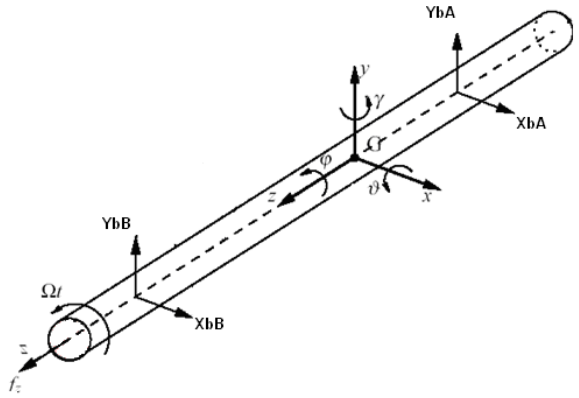

Fig. 2 Scheme of the Rotating Shaft

Supported by Two Radial Active Magnetic Bearings

II. MATHEMATICAL MODEL

The basic scheme of an active magnetic suspension is given in Fig. 1, wherein a rotating shaft is maintained according to a well-defined configuration by means of three magnetic bearings, two radial and one axial. Rotor shaft parameters are reported in Table I. The control of the configuration is carried out modulating the current supply to the magnetic bearings. Figure 2 shows the shaft, the centre of mass, the forces generated by the radial bearings, reference axes x, y, z, the Euler's angles $\vartheta, \varphi, \gamma$ and the reference sections A and B.

TABLE I
ROTOR SHAFT PARAMETERS

Symbol	Quantity	SI
m	Mass of rotor	144 kg
J_r	Inertia along x-y direction	26,87 kg m^2
J_a	Axial inertia	1,65 kg m^2
ε	Maximum value of the eccentricity of the mass center	4 10^{-6} m
χ	Principal inertia axis deviation	6 10^{-6}
n	Contingency coefficient	13

Since the radial behavior is independent on the axial behavior, there is no reason to complicate the mathematical model to implement the control law that stabilizes the radial position of the shaft.

Assuming that the shaft is a rigid body, the mathematical model of the whole system under analysis, with reference to the center of mass, is given by:

$$\mathbf{M}\frac{d^2\mathbf{q}}{dt^2}+\Omega\cdot\mathbf{G}\frac{d\mathbf{q}}{dt}=\mathbf{B}_\mathbf{q}\mathbf{f}(\mathbf{i}_\Delta,\mathbf{q}_\mathbf{b})+\mathbf{f}_\mathbf{g}+\mathbf{f}(\Omega t) \qquad (1)$$

where:

$$M=\begin{bmatrix} m & 0 & 0 & 0\\ 0 & J_r & 0 & 0\\ 0 & 0 & m & 0\\ 0 & 0 & 0 & J_r \end{bmatrix},\ \mathbf{G}=\begin{bmatrix} 0 & 0 & 0 & 0\\ 0 & 0 & 0 & -J_a\\ 0 & 0 & 0 & 0\\ 0 & J_a & 0 & 0 \end{bmatrix},$$

$$\mathbf{q}=\begin{bmatrix} x_g\\ \gamma\\ y_g\\ \vartheta \end{bmatrix},\ \mathbf{f}_\mathbf{b}=\begin{bmatrix} f_{xA}\left(i_{xA\Delta},x_{bA}\right)\\ f_{yA}\left(i_{yA\Delta},y_{bA}\right)\\ f_{xB}\left(i_{xB\Delta},x_{bB}\right)\\ f_{yB}\left(i_{yB\Delta},y_{bB}\right) \end{bmatrix},\ \mathbf{f}_\mathbf{g}=\begin{bmatrix} 0\\ 0\\ -mg\\ 0 \end{bmatrix}$$

(1a)

$$\mathbf{f}\left(\Omega t\right)=\Omega^2\begin{bmatrix} m\varepsilon\cos\left(\Omega t\right)\\ \chi\left(J_r-J_a\right)\cos\left(\Omega t\right)\\ m\varepsilon\sin\left(\Omega t\right)\\ -\chi\left(J_r-J_a\right)\sin\left(\Omega t\right) \end{bmatrix},$$

$$\mathbf{B}_\mathbf{q}=\begin{bmatrix} 1 & 0 & 1 & 0\\ -l_{bA} & 0 & l_{bB} & 0\\ 0 & 1 & 0 & 1\\ 0 & l_{bA} & 0 & -l_{bB} \end{bmatrix}$$

Considering the coordinate transformation:

$$\mathbf{q}_\mathbf{b}=\begin{bmatrix} x_{bA} & y_{bA} & x_{bB} & y_{bB} \end{bmatrix}^{\mathrm{T}}=\mathbf{B}_\mathbf{q}^{\mathrm{T}}\mathbf{q} \qquad (2)$$

the following model involving the displacements of sections A and B is obtained:

DOI 10.5963/JCET0201001

$$\mathbf{M_b}\ddot{\mathbf{q}}_\mathbf{b}+\Omega\mathbf{G_b}\dot{\mathbf{q}}_\mathbf{b}=\mathbf{f_b}+n\mathbf{B_q^{-1}f_g}+\mathbf{B_q^{-1}f}(\Omega t) \quad (3)$$

where the components of $\mathbf{f_b}$ are given by:

$$\begin{cases} f_{xA}=k_A\left[\left(\dfrac{i_1}{g_{0A}-x_{bA}}\right)^2-\left(\dfrac{i_2}{g_{0A}+x_{bA}}\right)^2\right] \\ f_{yA}=k_A\left[\left(\dfrac{i_3}{g_{0A}-y_{bA}}\right)^2-\left(\dfrac{i_4}{g_{0A}+y_{bA}}\right)^2\right] \\ f_{xB}=k_B\left[\left(\dfrac{i_5}{g_{0B}-x_{bB}}\right)^2-\left(\dfrac{i_6}{g_{0B}+x_{bB}}\right)^2\right] \\ f_{yB}=k_B\left[\left(\dfrac{i_7}{g_{0B}-y_{bB}}\right)^2-\left(\dfrac{i_8}{g_{0B}+y_{bB}}\right)^2\right] \end{cases} \quad (3a)$$

where:

$$k_A=1/4\,\mu_0N_A^2A_A\cos\alpha \quad k_B=1/4\,\mu_0N_B^2A_B\cos\alpha$$

n is a contingency coefficient and 2α is the angle between two successive magnetic poles (α=22°,5 in this work); g_{0A} and g_{0B} are the air gape of the two bearings A and B respectively (their values are reported in table II); i_i are the total currents in the coils of the electromagnet (they are four for every bearing). In Aeronautics the contingency coefficient "n" indicates how many times it must multiply the acceleration of gravity to obtain the acceleration of the airplane in the curvilinear path. In this work, as the rotor is part of the airplane, then it is subject to a contingency coefficient of force acting on its center of mass.

$\mathbf{M_b}$ and $\mathbf{G_b}$ are computed from $\mathbf{M}$ and $\mathbf{G}$ taking into account the change of variables:

$$M_b=\begin{bmatrix} \frac{Jr+lbB^2m}{(lbA+lbB)^2} & 0 & \frac{-Jr+lbAlbBm}{(lbA+lbB)^2} & 0 \\ 0 & \frac{Jr+lbB^2m}{(lbA+lbB)^2} & 0 & \frac{-Jr+lbAlbBm}{(lbA+lbB)^2} \\ \frac{-Jr+lbAlbBm}{(lbA+lbB)^2} & 0 & \frac{Jr+lbA^2m}{(lbA+lbB)^2} & 0 \\ 0 & \frac{-Jr+lbAlbBm}{(lbA+lbB)^2} & 0 & \frac{Jr+lbA^2m}{(lbA+lbB)^2} \end{bmatrix} \quad (3b)$$

$$G_b=\begin{bmatrix} 0 & \frac{Ja}{(lbA+lbB)^2} & 0 & -\frac{Ja}{(lbA+lbB)^2} \\ -\frac{Ja}{(lbA+lbB)^2} & 0 & \frac{Ja}{(lbA+lbB)^2} & 0 \\ 0 & -\frac{Ja}{(lbA+lbB)^2} & 0 & \frac{Ja}{(lbA+lbB)^2} \\ \frac{Ja}{(lbA+lbB)^2} & 0 & -\frac{Ja}{(lbA+lbB)^2} & 0 \end{bmatrix} \quad (3c)$$

Model (3) is nonlinear for the presence of magnetic forces $\mathbf{f_b}$. By means of linearization of these forces, the following model is obtained:

$$\mathbf{M_b}\ddot{\mathbf{q}}_\mathbf{b}(t)+\Omega\mathbf{G_b}\dot{\mathbf{q}}_\mathbf{b}(t)=\mathbf{K_s}\mathbf{q_b}(t)+\mathbf{K_I}\mathbf{i}_\Delta(t)+n\mathbf{B_q^{-1}f_g}+\mathbf{B_q^{-1}f}(\Omega t) \quad (4)$$

where:

$$\begin{cases} \mathbf{K_s}=diag(k_{xA},k_{yA},k_{xB},k_{yB}) \\ \mathbf{K_I}=diag(k_{ixA},k_{iyA},k_{ixB},k_{iyB}) \end{cases} \quad (4a)$$

$$\begin{cases} k_{xA}=k_{yA}=2k_A\dfrac{i_{0A}^2}{g_{0A}^3} \\ k_{xB}=k_{yB}=2k_B\dfrac{i_{0B}^2}{g_{0B}^3} \\ k_{ixA}=k_{iyA}=2k_A\dfrac{i_{0A}}{g_{0A}^2} \\ k_{ixB}=k_{iyB}=2k_B\dfrac{i_{0B}}{g_{0B}^2} \end{cases}$$

TABLE II
PARAMETERS OF THE CONTROL LAW

Symbol	Quantity	SI
$k_{xA}=k_{yA}$	Displacement gain of active magnetic bearing A	17 MN/m
$k_{xAB}=k_{yB}$	Displacement gain of active magnetic bearing B	7,2 MN/m
$k_{ixA}=k_{iyA}$	Current gain of active magnetic bearing A	5,6 kN/A
$k_{ixB}=k_{iyB}$	Current gain of active magnetic bearing B	2,3 kN/A
$I_{maxA}=I_{maxB}$	Maximum value of current	13 A
$i_{0A}=i_{0B}$	Bias current	6 A
$g_{0A}=g_{0B}$	Air gap	$2\ 10^{-3}$ m

The static load on bearing B turns out to be smaller than the static load on the bearing A, because it is more distant by the center of mass. The proportionality constant of the magnetic force k_a and k_b are placed in the numerator, then the gains of position and current of A are larger than B. Of course, these gains affect the control law because the gain of position premultiplies the four position components of the state vector, influencing the values of the array **A;** instead the array of current gains premultiplies the vector of inputs (current control), representing the input-state transition array **B**. Both the arrays **A** and **B** are essential to formulate the stabilizing solution of Lurie-Riccati for the formulation of the optimal control law.

As it is easy to verify, model (4) is unstable and consequently a suitable stabilizing control law has to be constructed. Putting:

$$\mathbf{z}(t)=\left[\mathbf{q}_\mathbf{b}^{\mathrm{T}}(t)\quad\dot{\mathbf{q}}_\mathbf{b}^{\mathrm{T}}(t)\right]^{\mathrm{T}} \quad (4b)$$

the state space form of (4) is given by:

DOI 10.5963/JCET0201001

$$\dot{\mathbf{z}}(t) = \mathbf{A}\,\mathbf{z}(t) + \mathbf{B}\,\mathbf{i}_{\Delta}(t) + \mathbf{B}_{\mathbf{d}}\left[\mathbf{f}_{\mathbf{g}} + \mathbf{f}\left(\Omega t\right)\right] \tag{5}$$

$$\mathbf{q}_{\mathbf{b}}(t) = \mathbf{C}\,\mathbf{z}(t) \tag{6}$$

where:

$$\mathbf{A} = \begin{bmatrix} \mathbf{0} & \mathbf{I} \\ \mathbf{M}_{\mathbf{b}}^{-1}\mathbf{K}_{\mathbf{S}} & -\mathbf{M}_{\mathbf{b}}^{-1}\mathbf{G}_{\mathbf{b}}\Omega \end{bmatrix},\ \mathbf{B} = \begin{bmatrix} \mathbf{0} \\ \mathbf{M}_{\mathbf{b}}^{-1}\mathbf{K}_{\mathbf{I}} \end{bmatrix} \tag{6a}$$

$$\mathbf{B}_{\mathbf{d}} = \begin{bmatrix} \mathbf{0} \\ \mathbf{M}_{\mathbf{b}}^{-1}\mathbf{B}^{-1} \end{bmatrix},\ \mathbf{C} = \begin{bmatrix} \mathbf{I} & \mathbf{0} \end{bmatrix}$$

III. OPTIMAL CONTROL LAW

In this paper we design a *LQR* control law of the shaft position. More precisely, the formulation of the control problem is: compute the control law $\mathbf{i}_{\Delta}(t)$ that minimizes the performance index:

$$J\left(\mathbf{z}(t), \mathbf{i}_{\Delta}(t)\right)_{LQR} = \int_0^{\infty} \left[\mathbf{z}(t)^T\,\mathbf{Q}\mathbf{z}(t) + \rho \mathbf{i}_{\Delta}(t)^T\,\mathbf{R}\mathbf{i}_{\Delta}(t)\right] dt \tag{7}$$

where $\mathbf{z}(t) = \left[\mathbf{q}_{\mathbf{b}}^{\mathrm{T}}(t) \quad \dot{\mathbf{q}}_{\mathbf{b}}^{\mathrm{T}}(t)\right]^{\mathrm{T}}$, subject to the constraint (5)-(6); $\mathbf{Q} \in R^{8\times 8}$ and $\mathbf{R} \in R^{4\times 4}$ are, respectively, positive semi-definite and positive definite matrices obtained by mean Bryson's rule according to [23] the matrix **Q** and **R** are respectively:

$$\mathbf{Q} = diag\left\{\frac{1}{\left(\max x_{bA}\right)^2}, \frac{1}{\left(\max y_{bA}\right)^2}, \frac{1}{\left(\max x_{bB}\right)^2}, \frac{1}{\left(\max y_{bB}\right)^2}, 0, 0, 0, 0\right\} \tag{8}$$

$$\mathbf{R} = diag\left\{\frac{1}{\left(\max i_{cAx}\right)^2}, \frac{1}{\left(\max i_{cAy}\right)^2}, \frac{1}{\left(\max i_{cBx}\right)^2}, \frac{1}{\left(\max i_{cBy}\right)^2}\right\} \tag{9}$$

where

$$\max x_{bA} = \max y_{bA} = \max x_{bB} = \max y_{bB} = 0.001\ m$$

$$\max i_{cAx} = \max i_{cAy} = \max i_{cBx} = \max i_{cBy} = 13\ A$$

Entries in the Q matrix, corresponding to the velocities when designing the LQR, are zero because the filling rule dictated by the references [14] is applied.

The solution of the problem is given by [15], [16]:

$$\mathbf{i}_{\Delta}(t) = -\mathbf{K} \cdot \mathbf{z}\left(t\right) \tag{10}$$

where $\mathbf{K} = \mathbf{R}^{-1}\mathbf{B}^{\mathrm{T}}\mathbf{S}$, **S** is the solution of the matrix Riccati's equation:

$$\mathbf{A}^T\mathbf{S} + \mathbf{S}\mathbf{A} - \rho^{-1}\mathbf{S}\mathbf{B}\mathbf{B}^T\mathbf{S} = \mathbf{0} \tag{11}$$

The expression (11) refers to algebraic Riccati's equation. In this equation we can see the matrix of the dynamic system depending on angular speed that causes coupling effects about displacements in radial directions. If we have to build up a speed-variant control, a continuous computing of stabilizing solution of **S** matrix must be taken into account. This could be very burdensome from a computational perspective because the controller must solve in few seconds a system of $n\left(n+1\right)/2$ equations.

This paper considers a different approach to develop a speed-variant optimal control the matrix **K** is obtained once the value of angular speed is known without solving that system of equation. This is obtained by a Matlab routine calculating each coefficient varying with the angular speed whose equation is carried out by a least squares curved fit as a second-order polynomial expression (it is executed clicking on the chart-Basic Fitting Tool and choosing the desired approximation and clicking on show equation). This leads to a control matrix **K** that is characterized by two block matrices (12), each is an algebraic matrix in the angular speed variable.

$$\mathbf{K} = \begin{bmatrix} \mathbf{K}_{\mathbf{q_b}} & \mathbf{K}_{\dot{\mathbf{q}}_{\mathbf{b}}} \end{bmatrix} \tag{12}$$

where:

$$\begin{cases} \mathbf{K}_{\mathbf{q_b}} = \Omega^2\mathbf{A}_{\mathbf{a}} + \Omega\mathbf{B}_{\mathbf{b}} + \mathbf{C}_{\mathbf{c}} \\ \mathbf{K}_{\dot{\mathbf{q}}_{\mathbf{b}}} = \Omega^2\mathbf{D}_{\mathbf{d}} + \Omega\mathbf{E}_{\mathbf{e}} + \mathbf{F}_{\mathbf{f}} \end{cases} \tag{12a}$$

Where $\mathbf{A_a}, \mathbf{B_b}, \mathbf{C_c}, \mathbf{D_d}, \mathbf{E_e}, \mathbf{F_f} \in R^{4\times 4}$

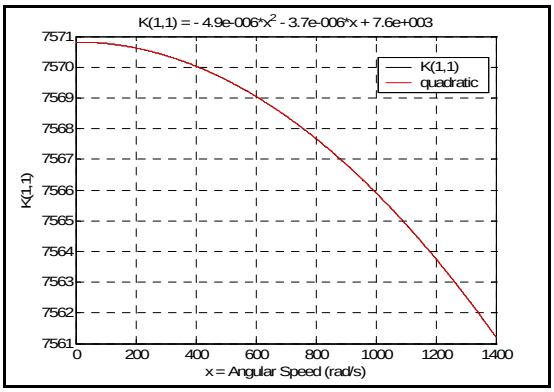

Fig. 3 Entry k_{11} vs Speed. The Red Line Denotes the Analytical Approximation.

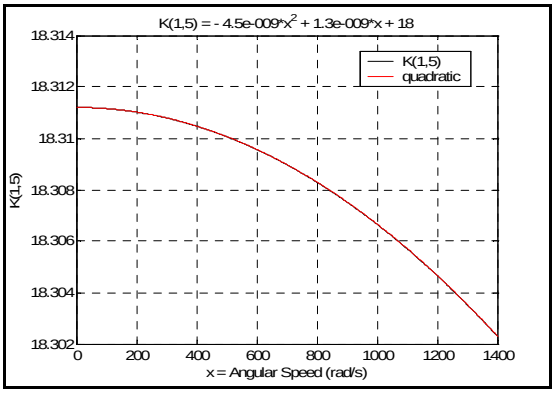

Fig. 4 Entry $k15$vs speed. The Red Line Shows the Analytical Approximation.

Figs. 3 and 4 show the shapes of two of the 32 elements of matrix **K**, together with their analytical expressions. These

DOI 10.5963/JCET0201001

were obtained in the Matlab environment by means of a curve-fitting procedure. The results of this procedure, when applied to all the entries of matrix **K,** show that the analytical approximation of these entries is at most a second-order polynomial. It follows that matrix **K** displays the structure reported in [17]. The resulting control law is given by:

$$\mathbf{i}_{\Delta}(t) = -\left[\mathbf{K}_{\mathbf{q_b}} \quad \mathbf{K}_{\dot{\mathbf{q}}_{\mathbf{b}}}\right]\left[\mathbf{q}_{\mathbf{b}}^{\mathrm{T}}(t) \quad \dot{\mathbf{q}}_{\mathbf{b}}^{\mathrm{T}}(t)\right]^{\mathrm{T}} \tag{13}$$

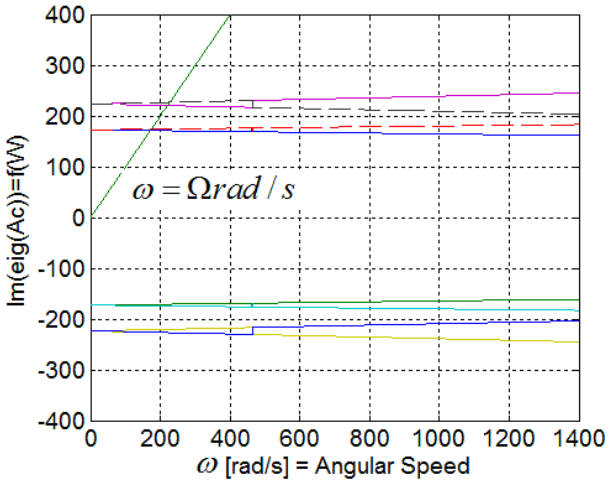

Fig. 5 Campbell Diagram with Speed-variant Optimal Control by Polynomial Approximation

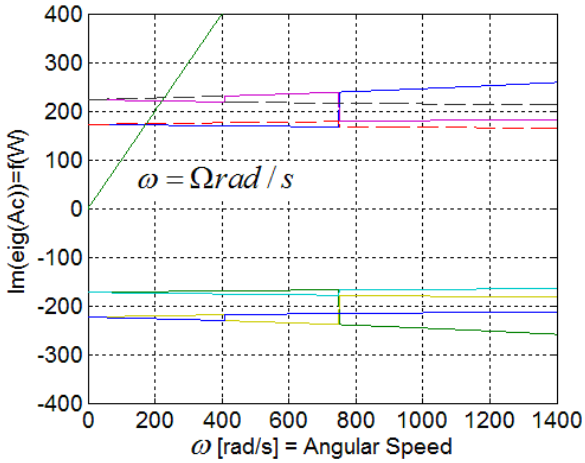

Fig. 6 Campbell Diagram Produced by a Control with Constant Gains at 0 Rad/s

The result is characterized by the same dynamic behaviour with a minimal computational burden of the controller as showed by plotting the Campbell diagram of the system for speed-variant optimal control by solving the ARE and one with constant gains set to 0*rad/s* shown in the Figures 5 and 6 respectively, [18]. In them J_a is the polar inertia moment of the shaft and J_r is its transverse moment. A constant control matrix can be used, because each sensor is located along each axis as to capture the displacements and speed signal along that axis. The elements out of the main diagonal of each block matrix constituting the entire matrix **K** are neglected to analyse the dynamic behaviour of the shaft during its rotation.

This technique was used in [17], with a lower value of rotor's mass and a difference of two order in polar moment of inertia. Coupling effects were measured in respect to the direction of gravity, according with the same direction of static acting load, along y-direction applied to the center of mass. The results show that in the presence of speed-variant optimal control, a displacement occurs along the x-direction. This displacement is caused by an increasing value of the control current due to the coupling effects of gyroscopic matrix as in the following expression:

$$i_i\left(q_{bj}, \dot{q}_{bj}, \Omega\right) = -\begin{bmatrix} \Omega^2\left(\sum_{j=1}^{4} a_{ij} q_{bj} + \sum_{j=1}^{4} d_{ij}\dot{q}_{bj}\right) + \\ \Omega\left(\sum_{j=1}^{4} b_{ij} q_{bj} + \sum_{j=1}^{4} e_{ij}\dot{q}_{bj}\right) + \\ \left(\sum_{j=1}^{4} c_{ij} q_{bj} + \sum_{j=1}^{4} f_{ij}\dot{q}_{bj}\right) \end{bmatrix} \tag{13a}$$

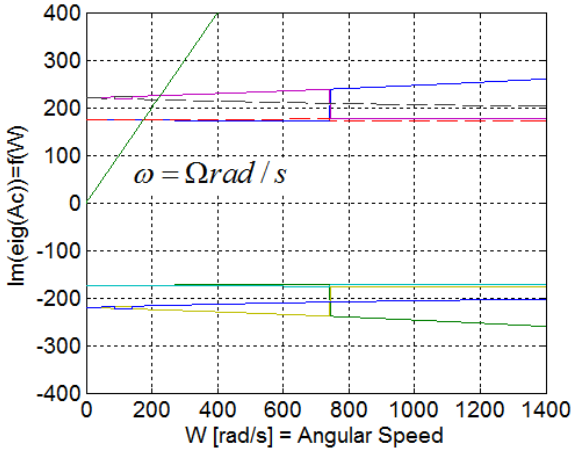

Fig. 7 Campbell Diagram Produced by a Control Matrix Set at 0*rad/s* and Characterized by Two Diagonal Block Matrix

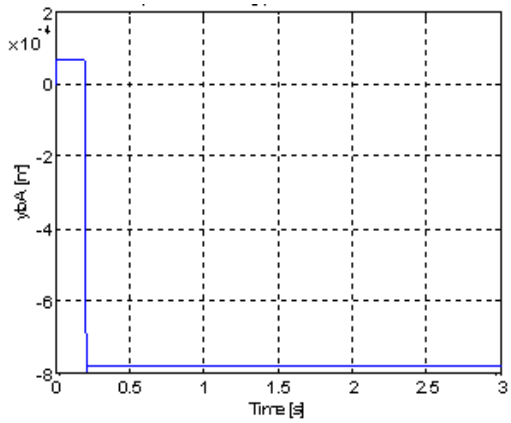

Fig. 8 Displacement of the Geometric Centre of Section A along y-direction

This means that the generic control current signal is generated by linear combination between the elements of

DOI 10.5963/JCET0201001

matrix and components of the state vector $\mathbf{z}(t)$ that causes displacements along the x-direction as fig. (7), (8) show.

In Figure 5, the step represented by the Campbell diagram is the same in Figures 6 and 7. The three steps in these figures say that there is a sudden change of rotational frequencies for the modes of precession. The step is smaller in Figure 5 because the optimal solution is obtained minimizing the values of angular velocity for which the sudden changes of the dynamic behavior may lead to instability in the rotating system. Both figures 6 and 7, considering a variation of the angular velocity of the rotor, are generated by a non-variable control law with the speed, then both the control laws are not the optimal solution of the model, and cause the rotor to transfer more energy during the sudden changes of the dynamic behavior; they are dictated by step highlighted by the eigen frequency, then it are at higher angular velocities.

The displacements along the orthogonal direction to the static acting load are not influenced by gyroscopic effects as happens in the case when variable gains are used. Control current signals show the same behaviour depending on variable or constant gains as shown in the figure (9) and (10) from [17], [18], [19] and [20].

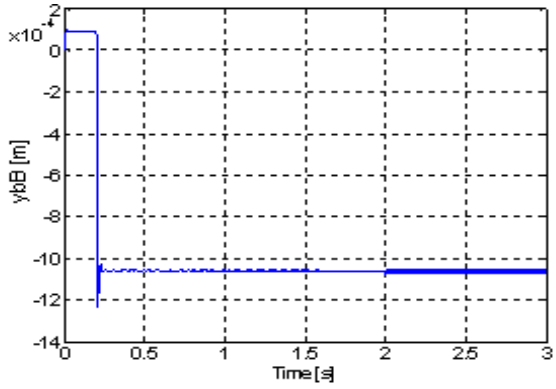

Fig. 9 Displacement of the Geometric Centre of Section B along y-direction

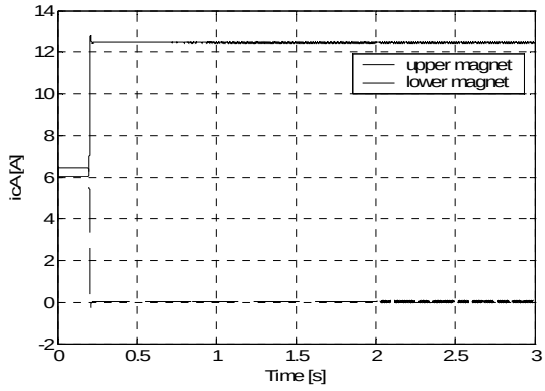

Fig. 10 Waveform of Currents Flowing in the Upper and Lower Electromagnets of Bearing A

However, a variable gain is introduced to show a different way to compute speed variant optimal control that is characterized by a similar dynamic behaviour to speed variant optimal control obtained by solving ARE (Algebraic Riccati Equation) and the produced control signal is obtained introducing only a value of angular speed rather than solving a complicated system of equations.

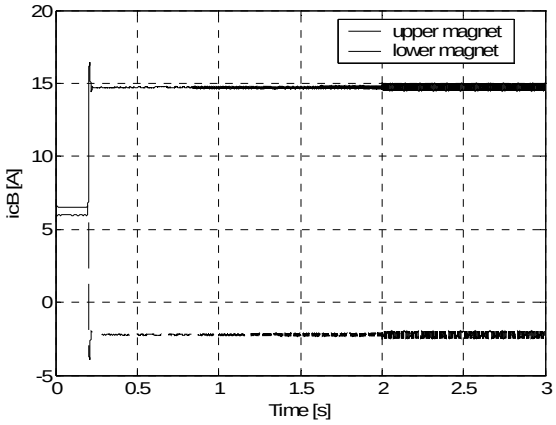

Fig. 11 Waveform of Currents Flowing in the Upper and Lower Electromagnets of Bearing B

This model of speed variant optimal control is more accurately named "sub-optimal" because of its similar dynamics with respect to the solving method of Riccati's equation, whose Campbell diagram is shown in figure 11.

IV. SIMULATION RESULTS

The closed loop model consisting of the model (5)-(6) and the control law (11) is now tested by means of simulation.

The simulations are carried out by the introduction of step input. It is introduced as exogenous excitation indentified by the gravity force, This acts at a certain time value in this paper, as shown in all figures at t equal to 0,2 s; the reason of the used step input is justified by the rapid movement of the aircraft during the fast rump up. In fact during the rapid climbing of aircraft, all the masses constituting the aircraft are subjected to a variation of acceleration. This is identified by n time the gravity force, where n is contingency coefficient, a typical parameter used in the structures design.

Table I shows that transverse moment of inertia is greater than one order than the polar moment of inertia. This data are obtained using a rotor having almost the same mass of the rotor installed in a Rolls Royce engine model used in military aircraft.

Figures 5 and 6 show the shape of imaginary parts of the eigenvalues of the closed loop dynamic matrix $\mathbf{A}-\mathbf{B}\,\mathbf{K}$ as it changes with rotor speed.

In order to test the effects of the control law (13), the model (4) is implemented in Matlab-Simulink software putting:

$$\mathbf{f}(\Omega t)=\Omega^2\begin{bmatrix} m\varepsilon\cos(\Omega t) \\ \chi(J_r-J_a)\cos(\Omega t) \\ m\varepsilon\sin(\Omega t) \\ -\chi(J_r-J_a)\sin(\Omega t) \end{bmatrix} \qquad (14)$$

Figs. 8 and 9 show the waveforms of the radial displacements of the geometric centres of sections A and B along the same direction of the gravity force (y-direction)

DOI 10.5963/JCET0201001

multiplied by *n* for simulating the rapid pull-up of the aircraft in presence of the harmonic load (12), assuming $\Omega = 700t$ *rad/s* for $t \in [0,2]$ and $\Omega = 1400$ *rad/s* for $t > 2$.

Examination of Figs. 8 and 9 reveals that sinusoidal oscillations arise during the shaft rotation along both x and y axes. The maximum displacement of the section centres occurs along y-axis due to the combined effects of the gravity, amplified by a contingency coefficient to simulate a fast pull-up of the aircraft, and harmonic load. However, both oscillation amplitudes and displacements are very small - less than $8 \times 10^{-4} m$.

The waveforms of the currents flowing in the coil windings of the active magnetic bearings are shown in Figs. 10 and 11. In each of the two figures there are two traces. A trace refers to the upper electromagnet of a bearing, whereas the other trace refers to the lower electromagnet of the same bearing. Examination of Figures 10 and 11 shows that in both bearings of sections A and B, the maximum current is less than the design value, equal to 13 A.

Considering [14], by setting the matrix **K** at zero, angular speed is built up to create stable levitation to develop the control of the shaft away from unstable phenomena. In this case matrix **K** has the structure:

$$\mathbf{K} = \begin{bmatrix} k_{11} & 0 & k_{13} & 0 & k_{15} & 0 & k_{17} & 0 \\ 0 & k_{22} & 0 & k_{24} & 0 & k_{26} & 0 & k_{28} \\ k_{31} & 0 & k_{33} & 0 & k_{35} & 0 & k_{37} & 0 \\ 0 & k_{42} & 0 & k_{44} & 0 & k_{46} & 0 & k_{48} \end{bmatrix} \quad (15)$$

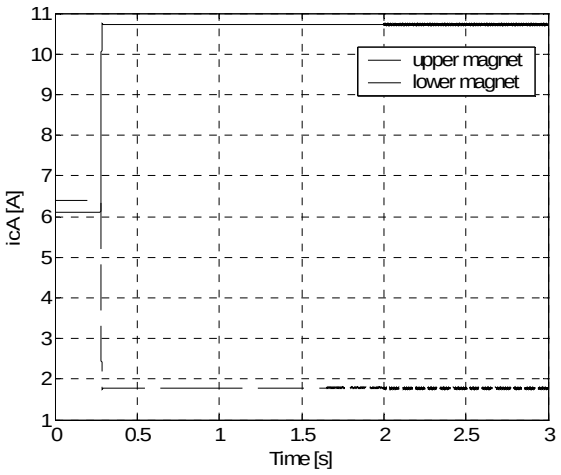

Fig. 12 Waveform of Currents Flowing in the Upper and Lower Electromagnets of Bearing A

(sub-optimal control at 0rad/s)

Figures 12 and 13 show the control current pathway.

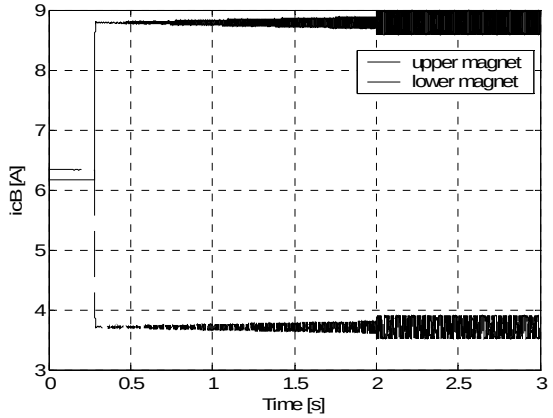

Fig. 13 Waveform of Currents Flowing in the Upper and Lower Electromagnets of Bearing B

(sub-optimal control at 0rad/s)

Now a simplification is considered: matrix (15) is set neglecting the elements outside the main diagonal of each block $R^{4\times4}$ so that to have matrix **K** structure as (16):

$$\mathbf{K} = \begin{bmatrix} k_{11} & 0 & 0 & 0 & k_{15} & 0 & 0 & 0 \\ 0 & k_{22} & 0 & 0 & 0 & k_{26} & 0 & 0 \\ 0 & 0 & k_{33} & 0 & 0 & 0 & k_{37} & 0 \\ 0 & 0 & 0 & k_{44} & 0 & 0 & 0 & k_{48} \end{bmatrix} \quad (16)$$

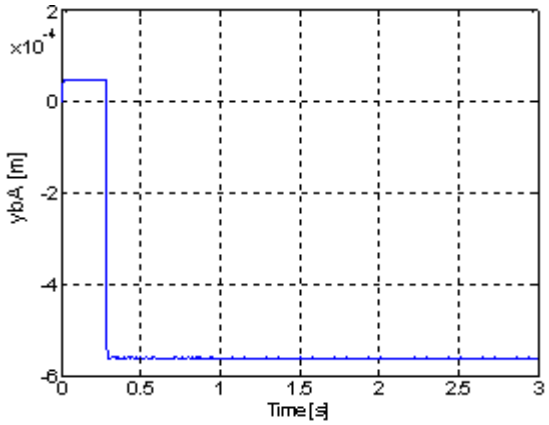

Fig. 14 Displacement of the Geometric Centre of Section A along y-direction

Results are shown in Figures 14 and 15 for the displacements, and Figures 16 and 17 for the control current.

TABLE III
DISPLACEMENT AND CONTROL CURRENT COMPARISON BY MATRIX K IN THE FORMS (12), (15) AND (16)

	K(12)	**K(15)**	**K(16)**
y_{bAmax}	-8 10^{-4} m	-55 10^{-4} m	-55 10^{-4} m
y_{bBmax}	-12 10^{-4} m	-3 10^{-4} m	-3 10^{-4} m
i_{cAmax}	13 A	10,5 A	10,5 A
i_{cBmax}	15 A	9 A	9 A

DOI 10.5963/JCET0201001

Table III shows that matrix (12) doesn't follow the condition of Brayson's rule because displacements are greater than one millimeter.

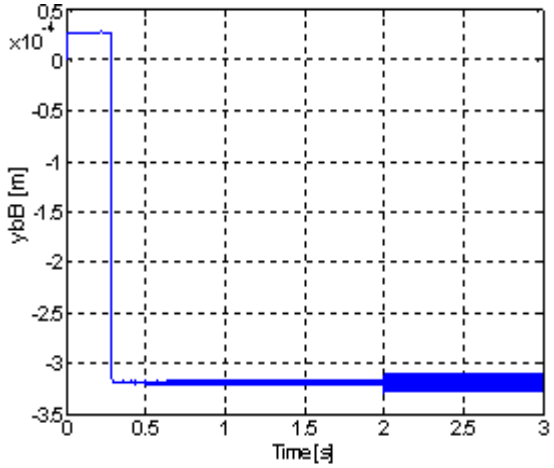

Fig. 15 Displacement of the Geometric centre of Section B along y-direction

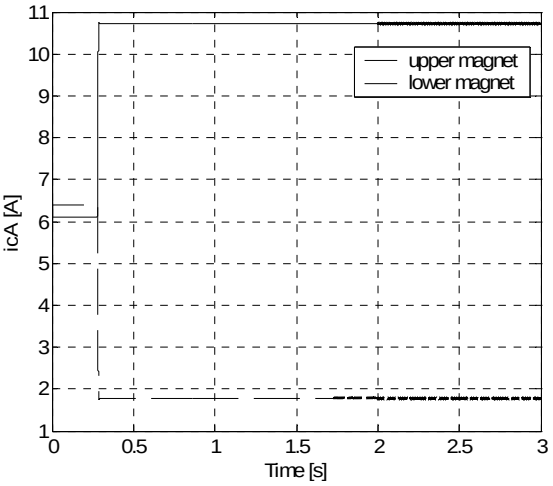

Fig. 16 Waveform of Currents Flowing in the Upper and Lower Electromagnets of Bearing A

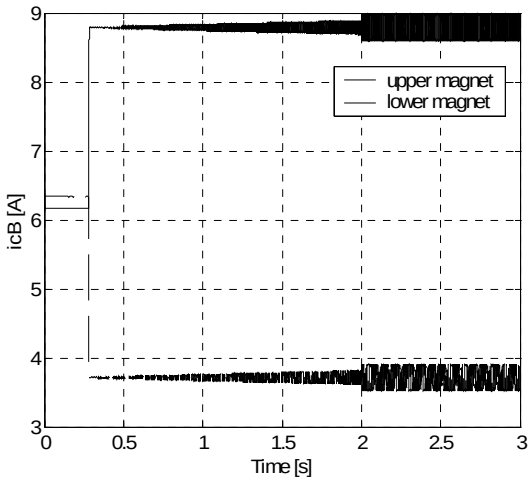

Fig. 17 Waveform of Currents Flowing in the Upper and Lower Electromagnets of Bearing B

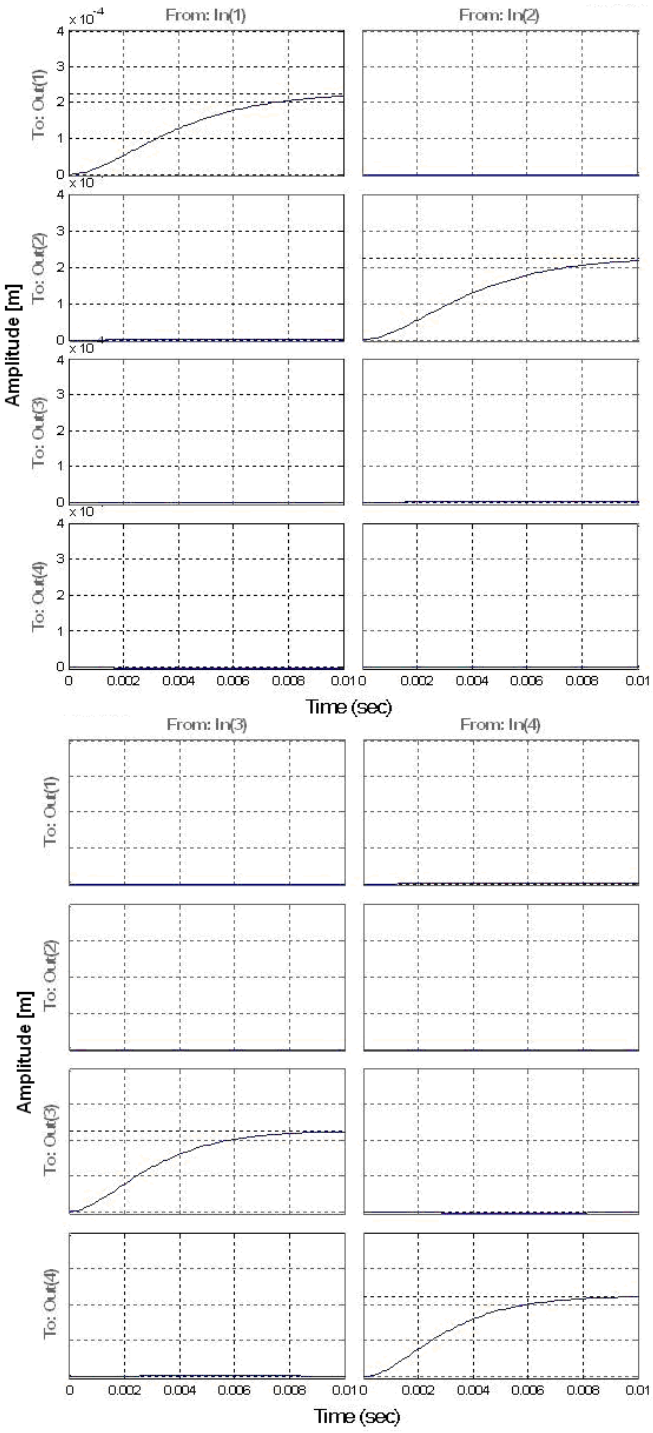

Fig. 18 Step Response of Transfer Function Matrix

It also happens for the control current; in fact, they are more thirteen ampere for the radial active magnetic bearing B. On the contrary, matrices (15) and (16) have similar behaviours in regard to displacements and control current. They are capable of maintaining displacements and control current signals around the values established by Brayson's rule. From this first comparison it seems that a speed varying matrix **K** given by relationship (16) produces displacements and control signals away from the design's values. Matrices in

DOI 10.5963/JCET0201001

the form (15) and (16) produce almost the same effects in terms of displacements and control currents.Now consider the transfer function matrix to analyse the performances of the turbojet shaft when it is subjected to the different control matrices (12), (15),and (16).

so that output is calculated as:

$$\mathbf{y}(s) = \mathbf{W}(s)\mathbf{u}(s) \tag{18}$$

where $\mathbf{u}(s)$ is the vector of the step input.

Varying the angular speed, the step response of the entire system with control matrix (12) is showed in Figure 18.

Only the elements along the main diagonal of the transfer function matrix show a relevant response to the step input varying with the angular speed. Others are small more than two orders as shown in Figure 19. Based upon the results shown in Figure 19 the same elements are neglected in order to obtain the rise time and settling time from the elements along the main diagonal.

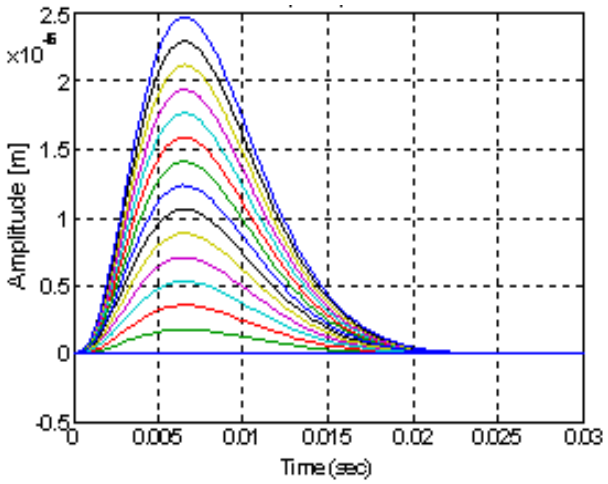

Fig. 19 Step Response of Transfer Function Elements out of Mean Diagonal of W(s)

TABLE IV
RISE TIME (T_Y) AND SETTLING TIME ($T_{z(2\%)}$) OF RESPONSE TO THE STEP INPUT VARYING CONTROL MATRIX (12) (15) AND (16)

	K(12)	K(15)	K(16)	
T_y [s]	0,00648	0,00663	0,00669	***Active Magnetic Bearing A***
$T_{z(2\%)}$ [s]	0,0107	0,011	0,011	
T_y [s]	0,00507	0,00499	0,00524	***Active Magnetic Bearing B***
$T_{z(2\%)}$ [s]	0,00844	0,00825	0,00883	

Table IV shows that the radial active magnetic bearing A, controlled using the control matrix (12), produces a lower rise time and lower settling time than one controlled by matrix (15) and (16). With regard to radial active magnetic bearing B using the control matrix (12), bearing B has a lower rise time than one obtained using the control matrix (16) but greater than one using (15). The settling time is lower than the one using the control matrix (16) but greater than one using (15).

Of course the simulation results should be proven by experimental data, but at present there is no plan of such a study.

V. CONCLUSIONS

The paper describes a speed-varying optimal control law developed for active magnetic suspension bearings used for sustaining a rotating shaft. Simulation shows that the proposed control laws are able to maintain the shaft in a stable levitation in the presence of static and harmonic loads. The simulations show that contactless motion between stator and rotor is guaranteed during the increasing of angular speed in presence of acting loads. Moreover, all the involved variables stay within their maximum design values except when using the first control matrix. Response to the step input shows that the radial active magnetic bearing A has a faster response and dynamic precision using the first control matrix rather than using the last two. The same can not be said for the bearing B, because it exhibits good performance in terms of rise time and settling at different control law, the settling is still faster than that of bearing A (table IV). This is because B is more distant from the center of mass and is therefore subject to a smaller static load, with a different dynamic behavior as a function of the control law.

However, the radial active magnetic bearing B shows good performances depending on the control matrix used. The future work should include a) the comparison of this control law with other control laws in the topic literature; b) make a comparative study between symmetrical bearing positions and asymmetrical bearing positions; and c) the instability analysis depending to the control law.

REFERENCES

[1] S. C. Mukhopadhyay, T. Ohji, M. Iwahara, and S. Yamada, " Modeling and Control of a New Horizontal-Shaft Hybrid-Type Magnetic Bearing, " IEEE Transactions On Industrial Electronics, vol. 47, no. 1, pp. 100–108, Feb. 2000.

[2] M. Komori, M. Kumamoto, and H. Kobayashi, "A Hybrid-Type Superconducting Magnetic Bearing System with Nonlinear Control," IEEE Transactions on Applied Superconductivity, vol. 8, no.2, pp. 79–83, June 1998.

[3] S. Sivrioglu and K. Nonami, "Sliding Mode Control With Time-Varying Hyperplane for AMB Systems"IEEE/ASME Transactions on Mechatronics, vol. 3, no. 1, pp. 51-59, Mar. 1998.

[4] F. Losch, C. Gahler, and R. Herzog, "Low Order µ- Synthesis Controller Design for a Large Boiler Feed Pump Equipped with Active Magnetic Bearing" in Proc. of IEEE International Conference on Control Applications, pp. 564–569, August 22-27, 1999, Hawai.

[5] Huettner, "Nonliner State Control of a Left Ventricular Assist Device (LVAD)" Proc. In 8th International Symposium On Magnetic Bearings, pp. 489-494, August. 26-28, 2002, Mito, Japan..

[6] E. M. Maslen, G. B. Bearnson, P. E. Allaire, R. D. Flack, M. Baloh, E. Hilton, et. al., "Feedback Control Applications in Artificial Hearts" IEEE Control Sys. Mag., vol. 18, no. 6, pp. 26–34, December. 1998.

[7] J. H. Lee, P. E. Allaire, G. Tao, J. Decker, and X. Zhang, "Experimental Study of Sliding Mode Control for a Benchmark Magnetic Bearing System and Artificial Heart Pump Susp ension", IEEE Transactions on Control System Technology, vol.11, no. 1, pp. 128–138, January 2003.

[8] J. X. Shen, K. J. Tseng, D. M. Vilathgamuwa and W. K. Chan, "A Novel Compact PMSM with Magnetic Bearing for Artificial Heart Application" Conference Record - IAS Annual Meeting (IEEE Industry Applications Society) 2, pp. 1201-1207, June 1994, Baltimore.

[9] F. Mohamed and I.B. Vishniac, "Imbalance Compensation and Automatic Balancing in Magnetic Bearing Systems Using the Q-Parameterization Theory", Conference Record - IAS Annual Meeting (IEEE Industry Applications Society) 2, pp. 2952–2957, June 1994, Baltimore.

DOI 10.5963/JCET0201001

[10] J. Delamare, O. Rulliiere, E. Yonnet and J. Paul, "Cardiac valve enhanced by permanent magnet" IEEE Transactions on Magnetics 29 (6 pt 2), pp. 3346-3348. 1993.

[11] T. R. Grochmal, A. F. Lynch, "Experimental comparison of nonlinear tracking controllers for active magnetic bearings", Control Engineering Practice 15 (1), pp. 95-107, Vol. 15, Issue 1, January 2007.

[12] J. Levine, J. Lottin, and J. C. Ponsart, "A nonlinear approach to the control of magnetic bearings" IEEE Transactions Control System Technology, vol. 4, no. 5, pp. 524–544, September 1996.

[13] T. Namerikawa and M. Fujita, "Modeling and robustness analysis of a magnetic suspension system considering structured uncertainties" in Proc. 36th IEEE Conference Decision Control, pp. 2559–2564, December1997, California.

[14] G. Schweitzer, H. Bleuler, and A. Traxler, Active Magnetic Bearings. ETH Zürich: Vdf Hochschulverlag AG an der ETH Zürich, 1994.

[15] H. Kwakernaak and R. Sivan, Linear Optimal Control Systems. NewYork: Wiley-Int., 1972.

[16] W. H. Kwon, A. M. Bruckstein, and T. Kailath, "Stabilizing statefeedback design via the moving horizon method" International Journal of Control, vol. 37, no. 3, pp. 234–239, 1982.

[17] G. Barbaraci, G. Virzi' Mariotti, "Controllo Sub-Ottimo per un Albero Rotante in Levitazione Magnetica Attiva", proceedings of XXXVIII AIAS Conference, September 9-11, 2009, Polytechnic of Turin.

[18] G. Genta - Consistent matrices in rotor dynamic. 1985 Meccanica 20 (3), pp. 235-248

[19] G. Curti, F. A. Raffa, F. Vatta, - An analytical approach to the dynamics of rotating shafts, 1992 Meccanica 27 (4) , pp. 285-292

[20] F. Sorge - Rotor whirl damping by dry friction suspension systems. 2008 Meccanica 43 (6), pp. 577-589

[21] J. T. Sawicki, E. H. Maslen, K. R. Bischof - Modeling and performance evaluation of machining spindle with active magnetic bearings - Journal of Mechanical Science and Technology Vol. 21 Issue: 6 Special Issue: Sp. Iss. SI Pages: 847-850, JUN 2007

[22] G. Schweitzer E. H. Maslen - Magnetic Bearings: Theory, Design and Application to Rotating Machinery, Springer editions, Zurich, January 2009.

[23] Bryson, Y. C Ho - Applied Optimal Control. Blaisdel Publishing Co. 1969

[24] Barbaraci G, Pesch A.H, Sawicki J.T (2010). "Experimental Investigations of Minimum Power Consumption Optimal Control for Variable Speed Amb Rotor". In Proceedings of the ASME 2010 International Mechanical Engineering Congress & Exposition IMECE2010 (pp.1-10). Vancouver, British Columbia.

Gabriele Barbaraci was born in Palermo on August 30 1978. He graduated with honors in aerospace engineering on April 2008. Actually he is Ph.D. on Mechanic Design with a thesis on Active Magnetic Bearings and a visiting student into Cleveland State University (USA) at Rotating Machinery Dynamic and Control laboratory for experimentation on active magnetic bearings system. He is Author of papers on application of control system on cancer cell's dynamic behavior and on dynamic systems on mechatronic devices.

Gabriele Virzi' Mariotti was born in Palermo on April 21, 1949. He graduated with praise in Mechanical Engineering on 1974, confirmed associate professor of Technique of Mechanical Building (with design) with the graduate course of Mechanical Engineering, and also professor of Vehicle Building, authors of more than hundred papers and two books. He is a reviewer of numerous International Journals, an evaluator of Italian Ministry of Education and Serbian Ministry of Education, and a coordinator of PhD in Mechanical Design of Palermo University.

DOI 10.5963/JCET0201001